EFFECT OF THERMOMECHANICAL PROCESSING ON FRACTURE TOUGHNESS AND DUCTILITY OF THE β-Ti-ALLOY Ti-10V-2Fe-3Al

G. Terlinde*, H.J. Rathjen**, K.-H. Schwalbe*, G.W. Kuhlman***

ABSTRACT

Fracture mechanics and tensile tests have been performed on the β-Ti-alloy Ti10V-2Fe-3Al. A variety of microstructures was established by several combinations of forging and heat treatment resulting in different types, morphologies and volume fractions of the α-phase. Both fracture toughness and ductility are reduced by the secondary α-phase, which precipitates from the matrix β-phase and controls the yield stress, but they also depend on the morphology of the primary α-phase and on grain boundary α. Based on a fractographic examination correlations between the microstructures and the mechanical properties were found.

INTRODUCTION

Metastable β-Ti-alloys show attractive combinations of ductility and fracture toughness for different strength levels [1-4]. Additional advantages are the good strength to density ratio and lower forging temperature compared to (α +β)-Ti-alloys. Furthermore, these alloys are deep hardenable so that homogeneous microstructures and properties can be achieved in thick sections.

β-Ti-alloys are forged at high temperatures and subsequently heat treated to establish the desired microstructures. These are characterized by the high temperature β-phase, from which various types of α-phase (primary α, secondary α, grain boundary α) can precipitate. The volume fractions, sizes, morphologies and the combinations of α-types are controlled by the forging and heat treating conditions [5-11]. It is known that such microstructure

*** Alcoa, Cleveland, USA
* Dept. of Materials Technology, GKSS-Research Center, Geesthacht, FRG.
** Industriewerke Karlsruhe-Augsburg, Karlsruhe, FRG.

variations can strongly influence the mechanical properties [1-4, 10-12]. Therefore, it is interesting to know which processing routes lead to microstructures with good properties or property combinations. For the forging components with a complex shape it is also important to know if the unavoidable local variations of the forging parameters affect the microstructures and properties, and if such property variations are acceptable.

Two of the important properties of β-Ti-alloys for commercial use are the fracture toughness and the ductility. Despite a considerable progress in the investigation of the microstructure/-property relationships there are still open questions especially with regard to a complete correlation between forging, heat treatment, microstructure and the micromechanisms of deformation and fracture. The goal of this study therefore, is to make a contribution to the understanding of the deformation and fracture behavior in the fracture mechanics and tensile test. A relatively new β-Ti-alloy, Ti-10V-2Fe-3Al, was chosen for the study. Based on earlier work [10-12] it was forged and heat treated such that different microstructures were established.

These varied in the size and volume fraction of secondary α, which mainly controls the yield stress, in the morphology and volume fraction of the primary α-phase and in the formation of subgrain- and grain boundary α; details will be presented later.

Fracture mechanics tests for the different microstructures were performed, and R-curves showing the resistance against stable crack growth were determined using both the K- and the J-integral concept. Special attention was paid to the crack growth resistance close to the initiation of stable crack growth (K_{Ic}, K_Q). For the above microstructures also tensile tests were performed. With the help of a detailed fracture analysis an attempt will be made to relate the observed properties to the various microstructures. Finally some conclusions for practical application will be drawn.

II. Experimental Methods

The majority of the alloy was produced by TIMET as bar material with a diameter of 250mm. In addition, a pancake forging was hot die forged by ALCOA from material supplied by RMI. The chemical compositions of the alloys are given in table 1. They are very similar, therefore, no effect from taking two heats was expected. During heat treatment contamination especially by oxygen was avoided by wrapping the specimens in Zr-foil and by using an argon atmosphere. For microscopy (optical, SEM, TEM) the specimens were prepared by grinding, polishing and etching, details are described elsewhere [11].

The fracture mechanics tests were performed on CT-specimens with a width of 30mm and a thickness of 7.5mm. For the tests on the pancake forging a thickness of 12.5mm was used. The specimens were prefatigued in air at 70Hz with an R-value of 0.1. The fracture mechanics tests were performed in air in displacement control at a travel-speed of 0.15mm/min. The crack extension Δa was measured by the DC-potential drop method using Johnson's equation [13]. From the data, which were collected by a computer, both $K_{Ic}(K_Q)$-values according to ASTM E399-81 as well as R-curves (K-Δa, J-Δa) were determined. The J-values were calculated according to the equation in ASTM E813-81. The initiation of stable crack growth has been described by the $K_{Ic}(K_Q)$-values and by K_o-values which were determined from the R-curves. With both values problems are associated. K_{Ic} is quite reproducible and easy to determine, but includes a certain amount of crack growth. This amount can be microstructure dependent and therefore, might not have a clearly defined relation to the real crack growth initiation. K_o therefore, is physically more appropriate, but its exact determination shows experimental problems, since the signals from the DC-potential drop method at crack growth initiation are influenced by crack tip blunting in a complex microstructure dependent way [14]. Both values have been determined in this study, and they show the same trends and ranking for the different microstructures and only differ in their values ($K_o < K_{Ic}$). Since K_{Ic} is also technically used it has been chosen for describing the results.

Tensile tests were performed on cylindrical specimens with a diameter of 4mm and a gage length of 20mm at a cross head speed of 1mm/min. The specimen surfaces were ground and polished before the test.

The fractography was mainly carried out by scanning electron microscopy (Philips SEM 505). Beside studying the fracture surface some CT-specimens were sectioned in the midthickness in order to examine the initiation and growth of microcracks in front of the main crack tip.

III. Results

1. Forging, Heat Treatment and Microstructures

The microstructures were established by high temperature forging and a subsequent double heat treatment as illustrated in a schematic phase diagram in figure 1. The only exception was a microstructure which was directly aged after forging. The higher heat treatment temperature controls the precipitation of primary α-phase (α_p) (10% at 775°C, 0% above the β-transus), at the lower heat treatment temperature the material is aged by the precipitation of secondary α particles, which are much finer than the pri-

mary α particles and control the yield stress of the alloy. The forging conditions affect the β-grain size and especially the morphology and size of the primary α-phase, and they can also influence the precipitation of grain bondary or subgrain bondary α. With these observations in mind and also based on recent work [11] a set of forging and heat treatment conditions was chosen which resulted in a variation of microstructure constituents, which were thought to be critical for fracture toughness. A summary is given in table 2.

Condition No. 1 is a microstructure with 10% α_p with an elongated morphology (figure 2a). It was established by high temperature forging which started in the β-field and finished high in the (α + β)-field, and it was followed by a solution treatment in the (α + β)-field at 775°C. Aging was performed at different temperatures between 400°C and 550°C to establish different yield stresses. For condition No. 2 the base material of condition No. 1 (without the heat treatment) was hot rolled at 680°C to a true strain of $\varepsilon = -1.2$ and then heat treated in the same way as condition No. 1. This resulted in a microstructure with a globular instead of an elongated α_p-morphology (figure 2 b). Condition 3 was established by β-solution treating the base material of condition 1 at 830°C, which gives a recrystallized microstructure without primary α and with a β-grain size of about 300μm (figure 2c). Similar aging treatments were performed as for the conditions No.1 and No.2. Beside the precipitation of secondary α (α_s) the formation of a continuous α-film along the β-grain boundaries occurs during aging. Since it is known that such a film can drastically affect the ductility and possibly the toughness, an additional condition without α_p, No. 4, was chosen in which the formation of a grain boundary film was suppressed. This microstructure was established by a forging process with direct aging.

2. Fracture Toughness

First the K_{Ic} result will be presented as a measure for the resistance against stable crack growth close to the initiation, then the R-curves showing the resistance also at further crack growth will be shown.

In figure 3 K_{Ic} (K_Q)-values are plotted versus yield stress for the two microstructures with different α_p-morphologies. With increasing yield stress that means with an increasing hardening by α_s-phase a drastic reduction in fracture toughness occurs for both α_p-morphologies leading to values around 30MPa $m^{\frac{1}{2}}$ at $R_{p0.2}$ = 1300MPa compared to 70MPA $m^{\frac{1}{2}}$ at 1100MPa. The K_{Ic}-values of the globular α_p-morphology are consistently lower than those for the elongated shape, the difference, however, is relatively small (3 - 4MPa $m^{\frac{1}{2}}$). A single data point is added which is taken from a different study [11], and it belongs to a microstructure with globular α_p in which in contrast to the microstructures described in

this study (condition 2) a thick, continuous α-film has developed along the subgrain bondaries (figure 2d). The presence of such a film apparently leads to a considerable toughness reduction. Figure 4 illustrates the K_{Ic}-results of the microstructures without α_p as a function of yield stress. The results for the microstructure with eleongated α_p are added as a reference curve. Condition No. 4 was only tested in a low strength condition. Again a severe toughness reduction occurs with increasing yield stress. Although there is no overlap of the data for both microstructures they seem to be on one curve. Compared to the microstructure containing 10% elongated α_p the K_{Ic}-values are very similar at yield stresses up to ≈1250MPa. At higher yield stresses the microstructure without α_p shows higher values, although it contains the grain boundary α-film.

The R-curve results were evaluated using K and J as fracture mechanics parameters. In case of linear elastic behavior K and J should be equivalent parameters related by the equation $K = \sqrt{EJ}$ (E: Young's Modulus). In reality elastic-plastic conditions apply but figure 5, in which K is plotted versus J for a low strength condition, shows that the deviation of K from the above relationship is only 8% at 2mm crack growth and about 2% at crack growth initiation. This deviation decreases with increasing yield stress, since linear elastic behavior is approached. Because of the relatively small error the R-curves will be presented with K as crack tip parameter. One could further reduce the error by using an effective K (K_{eff}) according to Irwin in which instead of the physical crack length an effective crack length including part of the plastic zone is taken.

In figure 6-8 the K-Δa-curve for the different microstructures are illustrated; in each diagram curves for different yield stresses are shown. The R-curve of the microstructure without α_p and grain boundary α (condition 4) is not included, because of the different specimen thickness effects on the R-curve had to be expected. As has been shown already by the $K_{Ic}(K_Q)$ values, an increasing yield stress reduces the K-values for the initiation of crack growth. In addition, it is apparent however, that also the slope of the R-curves - known as tearing modulus for J-Δa-curves - decreases at higher yield stresses.
This slope is not only depending on the hardening by secondary α but also on the other microstructure variations. Figure 9 shows K-Δa-curves for 3 microstructures ($\alpha_{pelong.}$, α_{pglob}, β-ST) at a comparable yield stress, and it is clearly visible that the microstructure with the elongated α_p shows a higher crack growth resistance than that with globular α_p, and in addition this diagram reveals that the highest crack growth resistance at this strength level is reached by the recrystallized microstructure with the grain boundary α-film. In order to quantify these results the slopes of the K-Δa-curves were evaluated for different yield

stresses and microstructures. Since most of the curves didn't show a constant slope, an arbitrary interval of crack growth between 0.2mm and 1.0mm was evaluated. The lower value was taken, because below Δa = 0.2mm problems with the reliability of the potential drop method have to be expected and around 1mm for several of the microstructures stable crack growth already ended. Despite taking an arbitrary crack growth interval and assuming a linear slope in this interval the effects of yield stress and microstructure can clearly be seen as illustrated in figure 10. The dK/da-values, however, should only be taken as semiquantitative, since slight variations are quite possible if the interval is varied.

The ranking of the slopes which was qualitatively described in figure 9, is apparently valid for all the yield stresses. It is interesting to note that the sensitivity of the slope dK/da to the yield stress is much smaller for the microstructures with globular α_p compared to those with elongated α_p or without α_p. The corresponding values at a yield stress of ~1190MPa are about 5, 10 and 20 MPa $m^{1/2}$/mm.

The ductility results for the above microstructures have been presented elsewhere [16], they will only be briefly summarized. The ductility drastically drops with increasing yield stress. In addition, the globular α_p- morphology gives higher ductilities than the elongated morphology which in turn shows better values than the β-solution treated condition with grain boundary α. Suppressing the grain boundary α results in a marked ductility increase with values close to those for the globular α_p-morphology.

3. Fractography

Studying the crack tips which had been prepared from the CT-specimens revealed that the macroscopic crack growth occured by the initiation, growth and coalescence of microcracks in front of the main crack (figure 11). Depending on the microstructure, however, different initiation sites were activated and also different growth paths were observed. For the microstructures with primary α the microcracks formed either at the interfaces between α_p and the aged matrix (figure 12a) or at the tripelpoints between α_p, aged matrix and subgrain boundary α-film (figure 12b). Crack growth was quite different, however, leading to a considerable crack deviation along the α_p interfaces for the elongated α_p (figure 13a) and to a much flatter growth through the aged matrix and along subgrain boundary α-film for globular α_p (figure 13b).

For the single microstructure with globular α_p but with a thick, continuous α-film showing a very low thoughness crack growth occurs to a much larger extent along the subgrain boundary α-film compared to the other microstructures with globular α_p (condition 2) (figure 13c).

With increasing yield stress a tendency to strain localization was observed. While at lower yield stresses a large portion of dimple type fracture was observed (figure 14a), at high yield stresses very localized deformation bands developed loading to a zig-zag like fracture surface (figure 14b).

The microstructures without α_p show crack growth initiation in the aged β-matrix even in the presence of a grain boundary-α-film (figure 15). In this case, however, after having crossed the first grain, the crack changes its path and further proceeds along the soft α-film. The microstructure without grain boundary α shows only transgranular crack growth.

IV DISCUSSION

The discussion will focus on relating the observed fracture toughness results to the forging and heat treatment conditions and to the microstructures, respectively. In addition possible effects on practical application will be described.

For an explanation of deformation and fracture one has to take into account that this alloy consists of two basically ductile phases, which both plastically deform. The combination of these two phases with respect to the types of α(α_p, α_s, subgrain - or grain-boundary-α) and their morphologies, size and volume fractions can vary strongly, which can lead to quite different local strain hardening, void nucleation and growth behavior.

A dramatic decrease of the crack growth resistance is caused by an increased degree of hardening by secondary α-phase (increasing yield stress), both for the crack growth initiation ($K_{Ic}(K_Q)$) and for further stable crack growth (figures 5 to 8). In this study and also in earlier work [11] with increasing yield stress a tendency to strain localization in the aged matrix has been observed (figure 14), leading to early crack nucleation at the interface of primary α where the deformation bands impinge. Two possibilities for the development of such deformation bands have been presented elsewhere [11,16,17], they are based on a high strength which is reached in the α_s-particles during plastic deformation leading to slip through the α_s/β-interfaces and to the formation of slip bands which finally link up to more macroscopic bands. A yield stress increase which is achieved by smaller α_s-particles is thought to lead to a more rapid strain hardening in the α_s-phase and to the formation of more localized slip which leads to void nuclation at smaller plastic strains. The ductility shows the same yield stress dependence as the fracture toughness. Despite basic differences between these tests (strain state e.g.) they have the varying strain localization in common, which seems to be the dominating effect of aging.

The elongated α_p-morphology results in a slightly higher crack growth resistance at the initiation and also at further stable crack growth. From the fractography (figure 13) it is apparent that the cracks are more deviated by the elongated α_p. From other studies it is known that such crack deflections lower the effective K_I-value [1,18]. The effect should depend on the length of the deflection, which in this study is controlled by the α_p length, and indeed results by Boyer and Kuhlman on Ti10-2-3 with different α_p-lengths support this conclusion [19].

In contrast to the fracture toughness the ductility is significantly lower for an elongated α_p-morphology compared to a globular shape. This observation has been studied in detail elsewhere [11], the main conclusion was that in the tensile test there is no benefit from crack deviation. In addition the long slip length of the elongated α_p favors early void nucleation, and the smaller interparticle spacing of the elongated α_p shortens the void growth phase.

Beside α_p and α_s the subgrain boundary α also can effect the crack growth resistance. This was shown on a microstructure with globular α, which was established by a forging route, that led to the same α_p-size as for the globular α_p described above, but which resulted in a thick, continuous α-film along the subgrain boundaries. In the presence of such an α-film a significantly reduced fracture toughness was found (figure 5).
Examination of the fracture process revealed that void formation in addition to the sites mentioned above was taking place at subgrain boundary tripel points, the proportion of crack growth along the film was markedly increased (figure 13a/c).
In an earlier paper by J. C. Williams et.al. [3] the grain boundary α-film had been assumed as a low energy crack path. Therefore, both from a viewpoint of an increased void density and an easy crack growth the low toughness results can be explained. In most of the studies on β-Ti-alloys no attention has been paid to a role of subgrain boundary α in the fracture process, and it is quite possible that in cases where a considerable toughness difference between elongated and globular α_p has been observed, some of this effect could be due to subgrain boundary α.

The microstructures without primary α show equal or better crack growth resistance compared to those with α_p (figure 5) even in the presence of a grain boundary α-film. While the grain boundary α leads to very low ductilities because of strain localization in the soft α-film, it has no detrimental effect on the fracture toughness, since at the initiation of stable crack

growth the crack advances transgranularly and therefore is not affected by the grain boundary α. The transgranular crack path is caused by the position of the prefatigue crack in the grain interior. After a small amount of stable crack growth of about 0.3mm

it is changing to a preferential crack growth along grain boundary α (figure 15).

The change to intergranular crack advance could be controlled by the grain boundaries which are reached by the crack and deviate it. But it is also possible that with an increasing plastic zone size void nucleation at grain boundary tripel points in front of the crack tip occurs leading to void coalescence along the α-film. This assumption is supported by the observation that at the specimen surfaces with larger plastic zone sizes (plane stress) the crack grows along the α-film from the beginning of stable crack growth. This is a very similar situation as with the microstructure containing globular α_p and a thick, continuous subgrain boundary α-layer. The important difference beside the α_p is the grain size (~10μm compared to ~300μm). For a small grain size the plastic zone can reach the grain diameter at or before the initiation of stable crack growth leading to void nucleation at grain boundary triple points in front of the crack tip. In addition it affects further crack grwoth, since the larger grain leads to much more crack deflection than the smaller grain size. This can explain the observation that for the large grains of the microstructures without α_p a rather steep increase of the K-Δa-curves was observed (figure 9), which overcompensates the effect of the low energy path. It also appears that a continuous α-film is necessary to lower the toughness.

From the results some conclusions can be drawn also with regard to possible applications of this alloy. It is essential not only to achieve a good fracture toughness but also guarantee a certain ductility. For the conditions tested in this study there is no microstructure which gives optimum values for both properties. It appears however, that the microstructure without α_p and grain boundary α (condition 4) has the relatively best combination of ductility and toughness. Further tests will have to show, however, if this is true also at higher yield stresses. The attractive properties are not too surprising, since this microstructure neither containes α_p as void nucleation site nor grain boundary α leading to strain localization and a low energy crack path.

If such a microstructure can be established in a component depends on its tolerance to variations in the forging parameters, since due to complex shapes local variations of these parameters cannot be avoided. For this reason and also for an improved general understanding more work on systematic correlations between forging parameters (temperature, strain, strain rate, cooling etc.) and the development of microstructures appears to be worth while.

CONCLUSIONS

Fracture mechanics and tensile tests were performed on the β-Ti-alloy Ti10V-2Fe-3Al. A variety of microstructures was established by different combinations of forging and heat treatment. These microstructures are characterized by the β-phase, from which α-phase precipitates leading to different α -types (primary $\alpha(\alpha_p)$, secondary α (α_s), subgrain or grain boundary α), to different volume fractions and morphologies as well as to various combinations of the α-types. From the fracture mechanics tests $K_{Ic}(K_Q)$-values and (K,J)-Δa-curves were determined. Fracture surfaces and crack tips were studied by scanning electron microscopy. The results can be summarized as follows:

(1) A yield stress increase by secondary α leads to a drastic reduction of the K- and J-values at the initiation of stable crack growth (K_o, J_o, K_{Ic}). The tearing modulus (dJ/ da, dK/da) is also reduced. The ductility shows the same trend. The reason was found to be a pronounced increase of strain localization in the aged matrix at higher yield stresses.

(2) An elongated α_p-morphology leads to higher K_{Ic}-values and to a higher tearing modulus compared to the globular shape. This effect is caused by a considerable crack deflection by the elongated α_p-morphology.

(3) For the microstructures containing α_p the fracture toughness is also affected by the α-phase precipitating at the subgrain boundaries. A thick, continuous α-film compared to a thin, not continuous α-film leads to a considerable toughness reduction. While in the first case the crack propagates mostly through the aged matrix, in the latter case crack growth occurs predominantly along the α-film, which is thought to be a low energy path.

(4) The microstructures without α_p have equal ($R_{p0.2} < 1250$MPa) or better ($R_{p0.2} > 1250$MPa) $K_{Ic}(K_Q)$ values compared to the microstructure with 10% elongated α_p even in the presence of grain boundary α. They also show the higher values for the tearing modulus. The initiation of stable crack growth takes place in the aged matrix in both microstuctures (with and without grain boundary α), so that a possible detrimental effect of grain boundary α is avoided. Amongst the two microstructures without α_p the condition without grain boundary α, however, appears much more attractive for commercial use, because in contrast to the microstructure with grain boundary α it shows

a much higher ductility, since the strain localization in the grain boundary α is avoided.

Acknowledgments

We would like to thank Mr. Grunwald and Mr. Bucher for their help in the experimental work and Prof. G. Lütjering for his contributions in the discussion.

REFERENCES

(1) F.H. Froes, R.F. Malone, J.C. Williams, M.A. Greenfield, J.P. Hirth, Alloys Design and Property Interrelations of Metastable Beta Titanium Alloys, in "Forging and Properties of Aerospace Materials" The Metals Society, 1977.

(2) T.W. Duerig, J.C. Williams: Overview: Microstructure and Properties of Beta-Titanium-Alloys, in "Beta Titanium Alloys in the 80's" ed. R.R. Boyer, H.W. Rosenberg, TMS-AIME, Warrendale, USA, 1984, p. 19-67.

(3) J.C. Williams, F.H. Froes, J.C. Chesnutt, C.G. Rhodes, and R.G. Berryman: ASTM STP 651, Toughness and Fracture Behavior of Titanium, 1978, p. 64.

(4) F.H. Froes, J.C. Chesnutt, C.G. Rhodes, and J.C. Williams: ASTM STP 651, Toughness and Fracture Behavior of Titanium, 1978, p. 115.

(5) R.R. Boyer: Journal of Metals, March 1980, vol. 32, p. 61.

(6) C.C. Chen and R.R. Boyer: Journal of Metals, July 1979, vol. 31, p. 33.

(7) G.W. Kuhlman, R. Pishko: Processing-Property Relationships in Hot Die Forged Alpha-Beta and Near Beta Titanium Alloys, in Proc. 5th Int. Conference on Titanium, Munich, Sept. 10-14, 1984, p. 469.

(8) I.W. Hall: Effect of Forging Variables on the Microstructure of Ti10V-2Fe-3Al, in "Proc. 5th Int. Conf. on Titanium", Munich, Sept. 10-14, 1984, p. 491.

(9) I. Weiss, F.H. Froes: The "Processing Window" for the Near Beta Ti10V-2Fe-3Al Alloy, in " Proc. 5th Int. Conf. on Titanium", Munich, Sept. 10-14, 1984, p. 499

(10)T.W. Duerig, G.T. Terlinde, and J.C. Williams: Metall. Trans. A., 11A, (1980), p. 1987.

(11)G.T. Terlinde, T.W. Duerig, J.C. Williams: Microstructure, Tensile Deformation and Fracture in Aged Ti10V-2Fe-3Al, Met. Trans. 14A (1983), p. 2101.

(12)G.T. Terlinde et.al.: The Effect of Heat Treatment on Microstructure and Tensile Properties of Ti10V-2Fe-3Al, in "Proc. of 4th Int. Conf. on Titanium, Kyoto, Japan, May 19-22, 1980, Vol. 2, p. 1571.

(13)K.-H. Schwalbe, D. Hellmann: Application of the Electrical Potential Method to Crack Length Measurements Using Johnson's Formula, J. of Testing and Evaluation, May 1981, p. 218.

(14)J. Heerens, K.-H. Schwalbe, D. Hellmann, J. Knaack, J.Müller-Roos: Application of the DC-Potential Drop Method and the Partial Unloading Methods to Fracture Mechanics Tests, GKSS-Report, 85/E/16.

(15)G. Terlinde, H.J. Rathjen, G.W. Kuhlman, G. Lütjering: Microstructure, Fracture Toughness and Ductility in the Beta-Titanium Alloy Ti10V-2Fe-3Al, submitted to Met. Trans.

(16)T. Hamajima, G. Lütjering, and S. Weissmann: Met. Trans, 4, (1973), p. 847.

(17)M. Young, E. Levine, and H. Margolin: Metall. Trans. A, 10A, (1979), p. 359.

(18)S. Suresh: Crack Deflection: Implications for the Growth of Long and Short Fatigue Cracks, Met. Trans. 14A (1983), p. 2375.

(19)R.R. Boyer, G.W. Kuhlman: Processing-Properties Relationships of Ti10V-2Fe-3Al, Presentation at TMS-AIME-FAll Meeting, Oct. 13-17, 1985, Toronto.

TABLE 1 Chemical Composition of the Alloys

	V	Fe	Al	O	N	C	Ti
Timet	9.3	1.8	3.2	0.082	0.01	0.03	Bal.
RMI	9.7	1.8	3.2	0.075	0.01	0.03	Bal.

TABLE 2 Forging, Heat Treatments and Microstructures

Condition	Forging	Heat Treatment	Microstructure
1	β + α/β	Solution Treatment at 775°C Aging Treatment between 400°C and 550°C	10% α_p elongated Various α_s size and amount
2	$\beta+\alpha/\beta$ like Condition 1 + rolling at 680°C(ε=-1.2)	— " —	10% α_p globular Various α_s-size and amount
3	$\beta+\alpha/\beta$ like Condition 1	Solution Treatment at 830°C Aging Treatment like Cond. 1+2	0% α_p Grain boundary α-film. Various α_s-size and amount
4	Forging + direct aging	----------	0% α_p No grain boundary α. Various α_s size and amount

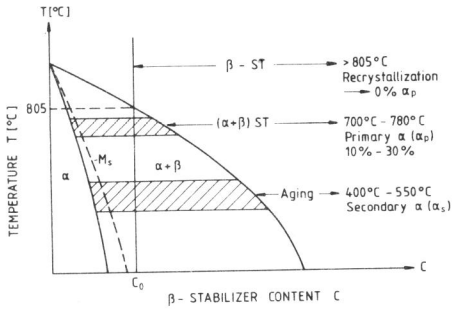

Fig. 1 Schematic Phase Diagram of β–Ti–alloy

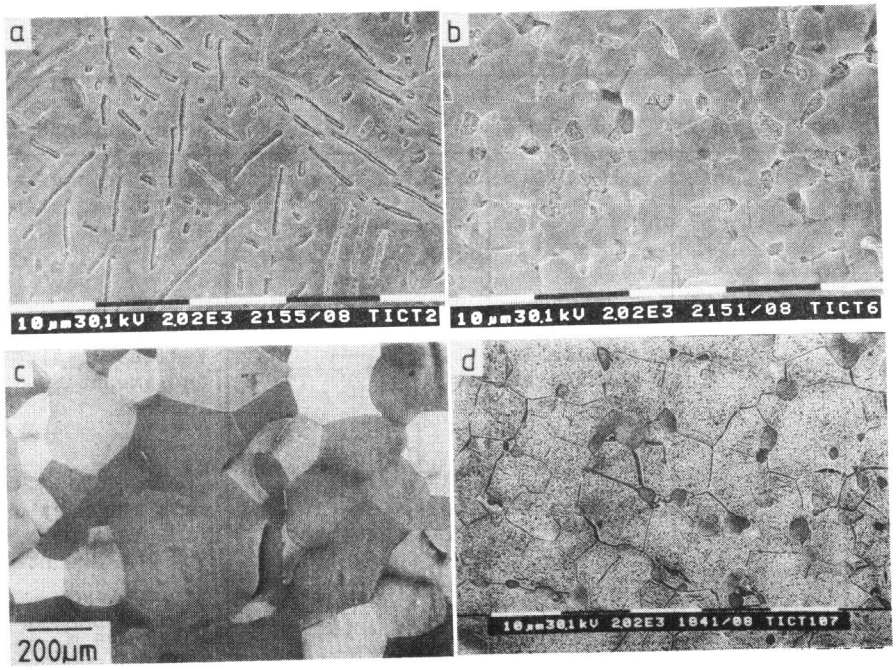

Fig. 2 Different Microstructures (SEM)

a) 10% elongated α_p, b) 10% globular α_p
c) 0% α_p (β–solution treated + aged, grain boundary α)
d) 10% globular α_p, thick continuous subgrain boundary α

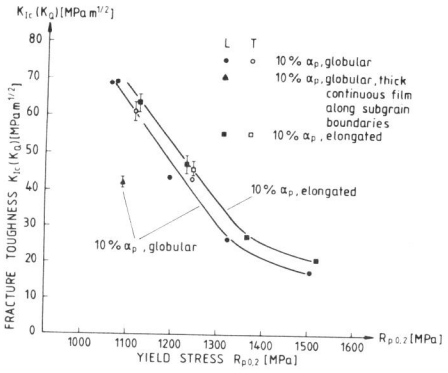

Fig. 3 K_{Ic} (K_Q) as a function of yield stress for different α_p-morphologies

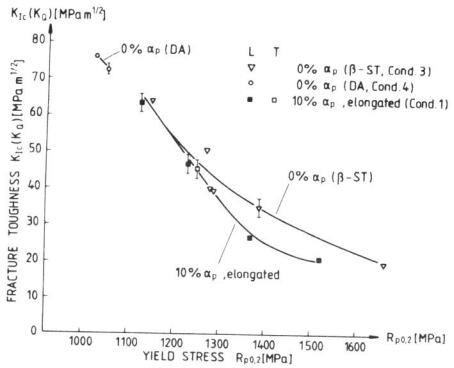

Fig. 4 K_{Ic} (K_Q) as a function of yield stress for microstructures without α_p

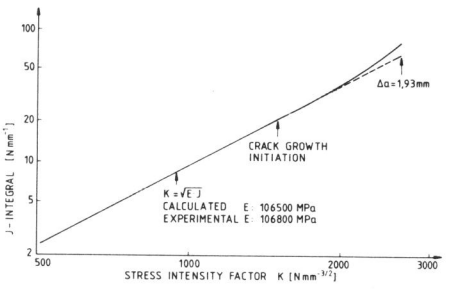

Fig. 5 J versus K, $R_{p0.2}$ 1100MPa

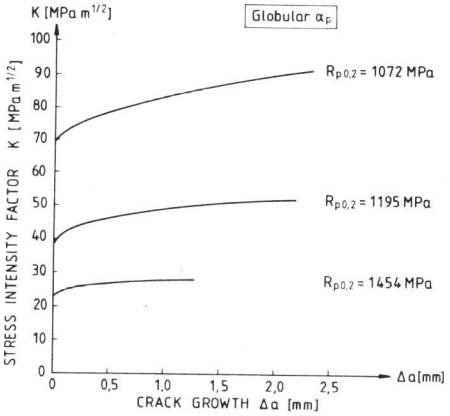

Fig. 6 K-R-curves for globular α_p different yield stresses

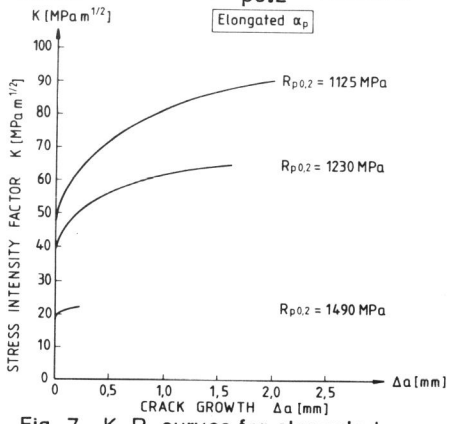

Fig. 7 K-R-curves for elongated α_p different yield stresses

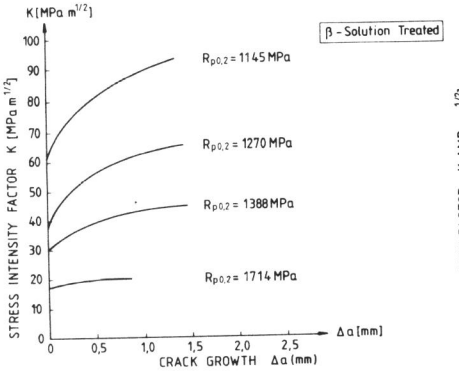

Fig. 8 K-R-curves for β-solution treated cond.(0%) α_p) different yield stresses

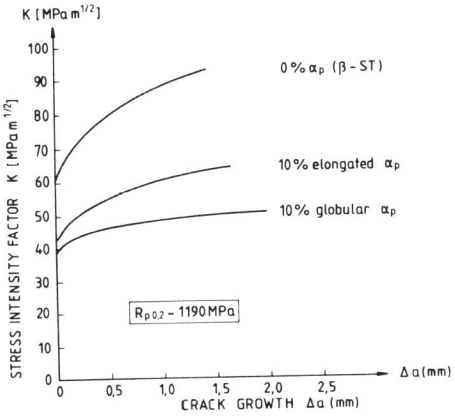

Fig. 9 K-R-curves for different microstructures, $R_{p0.2} \sim 1190$MPa

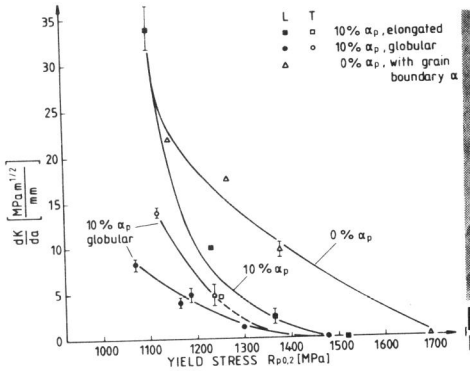

Fig. 10 Tearing modulus (dK/da) for different microstrustures and yield stresses

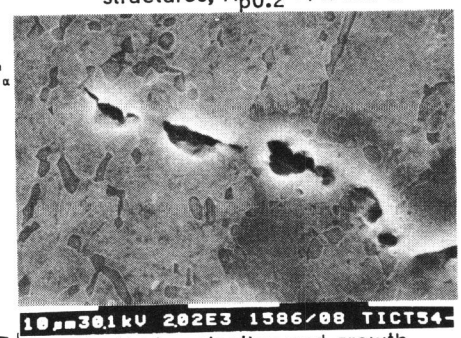

Fig. 11 Void nucleation and growth in front of a crack tip (SEM)

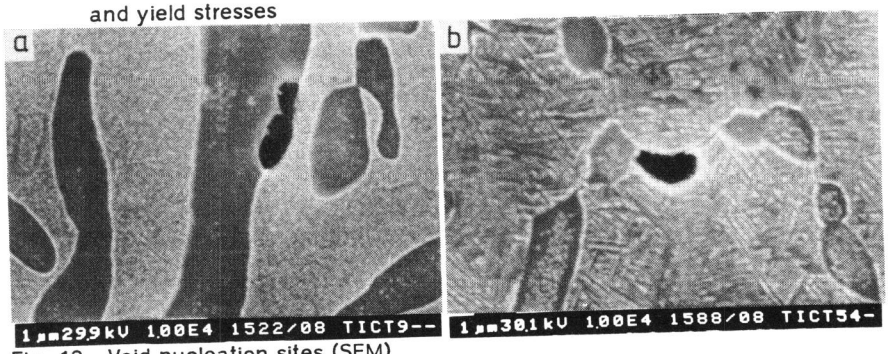

Fig. 12 Void nucleation sites (SEM)

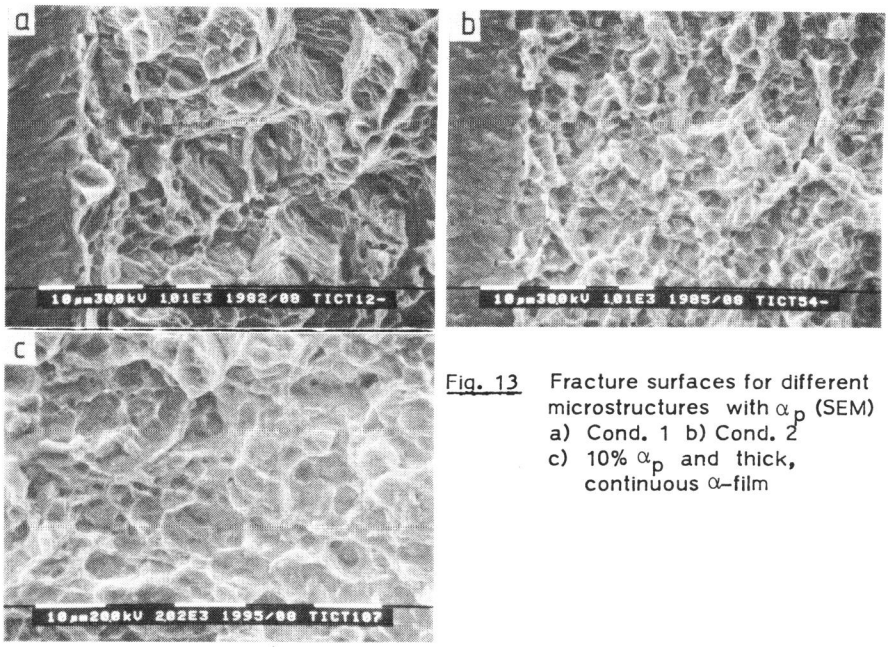

Fig. 13 Fracture surfaces for different microstructures with α_p (SEM)
a) Cond. 1 b) Cond. 2
c) 10% α_p and thick, continuous α–film

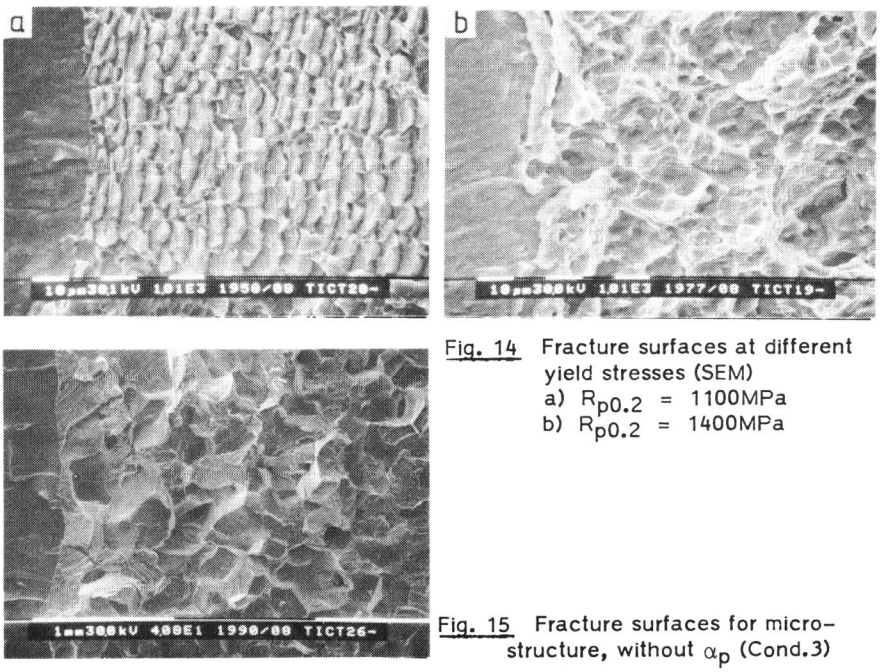

Fig. 14 Fracture surfaces at different yield stresses (SEM)
a) $R_{p0.2}$ = 1100MPa
b) $R_{p0.2}$ = 1400MPa

Fig. 15 Fracture surfaces for microstructure, without α_p (Cond.3)